Beyond the timedependent Hartree grid approximation for curvecrossing problems

Jose CamposMartinez, Janet R. Waldeck, and Rob D. Coalson

Citation: J. Chem. Phys. **96**, 3613 (1992); doi: 10.1063/1.461914
View online: http://dx.doi.org/10.1063/1.461914
View Table of Contents: http://jcp.aip.org/resource/1/JCPSA6/v96/i5
Published by the AIP Publishing LLC.

Beyond the time-dependent Hartree grid approximation for curve-crossing problems

Jose Campos-Martinez,[a] Janet R. Waldeck, and Rob D. Coalson[b]
Department of Chemistry, University of Pittsburgh, Pittsburgh, Pennsylvania 15260

(Received 29 July 1991; accepted 16 October 1991)

A new "configuration-interaction" method is presented which extends the single-surface time-dependent Hartree grid (TDHG) approximation into a formally exact algorithm for obtaining multidimensional quantum wave-packet dynamics on nonradiatively coupled electronic potential surfaces. As a numerical example, photofragmentation cross sections are computed for a two-degree-of-freedom model of direct dissociation. For systems prepared in vibrationally excited states of the ground electronic potential the TDHG approximation fails due to "direct correlation" effects, while our method provides accurate results.

I. INTRODUCTION

The role of wave-packet theory in computing and interpreting quantum-dynamical properties continues to grow at a rapid pace.[1] Central to this growth is the availability of reliable and efficient numerical techniques for simulating the quantum evolution of chemically interesting molecular systems. Despite considerable progress in the development of such technology, there is still no general algorithm for performing exact Schrödinger evolution of nuclear wave packets on a prescribed potential-energy surface that can be applied to systems with more than three degrees of freedom. Hence, even exact gas-phase tetra-atomic dynamics is currently at the edge of tractability.

The situation for polyatomic and condensed-phase quantum systems is not so bleak as the opening paragraph implies if we are willing to settle for approximate solutions to the Schrödinger equation. One approach which has received considerable attention recently is the time-dependent Hartree (TDH) method [also known as the time-dependent self-consistent-field (TDSCF) method],[2] in which the complete system wave packet is factorized into a product of single-degree-of-freedom packets and each one-dimensional factor evolved in its own one-dimensional "variationally optimized" effective potential. For problems involving motion on a single Born–Oppenheimer (BO) potential surface, the effective potential for each degree of freedom is obtained by averaging the many-body interaction potential over the instantaneous probability distribution of all the other degrees of freedom. In this way, certain aspects of interdimensional coupling, such as mode–mode energy transfer, are reasonably well accounted for. Indeed, the TDH approximation has proved useful for studying a number of short-time (subpicosecond) photodissociation and inelastic molecular scattering processes.[2,3] Nonetheless, the TDH factorization of the overall system wave packet omits "direct correlation" effects, i.e., features which depend directly on the nonfactorizability of the exact multidimensional wave packet.

In order to study processes involving long-lived (multipicosecond) complexes with more complicated dynamical signatures (such as double-well tunneling), numerical investigation[2–4] indicates that it will be necessary to go beyond the TDH approximation and include direct correlation effects neglected at the TDH level. Recently, we introduced[4] a configuration-interaction (CI) algorithm which enables direct correlation to be included by expressing the exact system wave function as a time-dependent superposition of factorized, TDH-type basis functions. Substitution into the Schrödinger equation leads directly to equations of motion for the superposition coefficients responsible for mixing the basis functions. Through the time development of these coefficients, details of the overall system wave function which cannot be described via a single product of one-dimensional functions are recovered.

The notion of improving upon the TDH approximation to the Schrödinger wave-packet evolution by "mixing" several approximate TDH level solutions is not new. It is, of course, a time-dependent analog of the (static) self-consistent-field configuration-interaction (SCF-CI) procedure which lies at the heart of modern molecular electronic structure theory.[5] Time-dependent CI algorithms for problems of nuclear dynamics of distinguishable particles on given potential-energy surfaces are at a much more primitive stage of development.[4,6] The novel features of our algorithm stem from a desire to streamline the computation of CI corrections to the TDH level dynamics. To this end, we maintain a time-dependent orthonormal basis set of one-dimensional wave functions in each coordinate in a simple way by propagating all product basis functions according to the *same* effective separable potential. Not only do the evolving basis functions remain factorizable and orthonormal, but computational labor in constructing the basis set grows strictly linearly with spatial dimensionality. In the case of motion on a single potential surface the appropriate separable potential is generated by an application of the TDH prescription to one "central" wave packet in the initial collection of basis packets (typically the nodeless wave packet upon which an orthonormal set of "excited states" is initially constructed).

[a] Fulbright Fellow, 1989–1991; permanent address: Instituto de Fisica Fundamental, Centro Mixto, Consejo Superior de Investigaciones Cientificas, Serrano 123, E-28006 Madrid, Spain.

[b] Camille and Henry Dreyfus Teacher-Scholar.

 0021-9606/92/053613-11$06.00

As demonstrated in Ref. 4 (henceforth referred to as Paper I), this procedure enables the construction of a traveling orthonormal basis set which is flexible enough to represent complicated wave forms that can arise in scattering and photodissociation applications. Furthermore, for problems of the type considered in Paper I the CI part of the algorithm converges rapidly and reliably.

In this paper we extend the wave-packet CI algorithm introduced in Paper I to treat motion on two (or, in principle, more) nonradiatively coupled potential-energy surfaces. The concept of coupled-surface dynamics finds application in several experimental contexts.[7] One important example entails a molecular transition between different electronic states in a region of nuclear coordinate space where the BO potential surfaces associated with those electronic states are nearly degenerate. Such curve crossing is common in electronic excited-state processes (stimulated and probed in great detail by various optical spectroscopies[7]), so useful theoretical modeling of excited-state dynamics depends critically on our ability to compute curve-crossing effects accurately and efficiently.

The theoretical intrigue of curve-crossing dynamics stems in part from its inherent nonclassicality. Even when the intersurface coupling is precisely specified (cf. Sec. II), there is no way to guess from classical mechanics alone the probability that a molecule will "hop" from one electronic state to another when its nuclear coordinates go through a crossing seam in the relevant BO potential surfaces. Furthermore, when these nuclear coordinates are represented in a more complete way by wave-packet states, it is not obvious (without the benefit of examples provided by exact wave-packet propagation codes!) how a packet will behave when it goes through such a crossing seam, and in particular what wave form will be created on the originally unoccupied surface. From the point of view of extending the single-surface CI algorithm presented in Paper I, the challenge is to isolate a "best zeroth-order" (time-dependent) Hamiltonian H_0, which generates a perpetually orthonormal set of two-surface spinor-type basis functions in a simple manner. To do this we have identified "best diabatic" guiding potentials on which to propagate the spatial wave packets on each surface. These potentials are real and Hartree type (i.e., separable), so the basis-set orthonormality is automatically maintained.

We have isolated two candidates for the "best diabatic" guiding potentials. They are set forth in Secs. IV A and IV B, after the mathematical problem of interest is introduced and motivated in Sec. II, and the general strategy of our CI scheme is presented in Sec. III. Then in Sec. V we demonstrate the utility of coupled-surface wave-packet CI by a numerical application involving a two-degree-of-freedom model of curve crossing in molecular photodissociation processes. Specifically, we consider the nonradiatively coupled Beswick–Jortner potential surfaces[8] recently studied within the TDH approximation in Ref. 9 (henceforth referred to as Paper II). We find, as in earlier work on single-surface problems,[3(b),4] that spatially extended wave packets associated with excited vibrational eigenfunctions (which arise, for example, in studying photodissociation of vibrationally excited molecules) are not always easily handled by simple TDH methods. The two-surface CI algorithm of Sec. IV is found to accurately and efficiently incorporate the "direct correlation" effects which elude TDH level dynamics. Both candidates for "best diabatic" potential surfaces prove effective, and their relative merits are compared. The paper concludes with a Discussion and Conclusion (Sec. VI), in which strengths, weaknesses, and possible extensions of the proposed approach are discussed.

II. WAVE-PACKET DYNAMICS FOR CURVE-CROSSING SYSTEMS

For a system consisting of two coupled diabatic potential-energy surfaces, the Hamiltonian governing the motion can be written as[10]

$$H_e = H_1 |e_1\rangle\langle e_1| + H_2 |e_2\rangle\langle e_2| + G(|e_1\rangle\langle e_2| + |e_2\rangle\langle e_1|), \tag{2.1}$$

where $|e_{1,2}\rangle$ are (structureless) diabatic electronic states, $H_{1,2}$ are the corresponding Hamiltonians for motion on the isolated diabatic surfaces $V_{1,2}$, and G is the coupling function responsible for transitions between diabatic surfaces. We will term G the "nonradiative coupling" function because it prescribes a nonradiative mechanism for transitions between zeroth-order diabatic electronic states. Specializing to the simplest multidimensional case, i.e., for a system with two spatial degrees of freedom, these terms can be written for surface 1 (and analogously for surface 2) as

$$H_1 = h_{1x} + h_{1y} + U_I^{(1)}(x,y). \tag{2.2}$$

Here, h_{1x} is a "single-particle" Hamiltonian, $h_{1x} = T_x + v_{1x}(x)$; T_x is the kinetic-energy operator (with $\hbar = 1$ here and throughout the paper) $T_x = -(1/2m_x)\partial_x^2$, and v_{1x} is the "single-particle potential" for the x motion on surface 1. h_{1y} is defined analogously. The interaction potential on surface 1 is given by $U_I^{(1)}(x,y)$. Combining this term with the single-particle potentials $v_{1x}(x)$ and $v_{1y}(y)$ yields an expression for the overall diabatic potential surface 1,

$$V_1(x,y) = v_{1x}(x) + v_{1y}(y) + U_I^{(1)}(x,y). \tag{2.3}$$

For simplicity, we assume a factorizable form for the interaction potential, $U_I^{(1)}(x,y) = u_{1x}(x)u_{1y}(y)$, and also for the coupling function, $G(x,y) = g_x(x)g_y(y)$. Thus the Hamiltonian is completely specified.

A general two-component excited-state wave packet can be described as

$$|\Psi(t)\rangle = \phi_1(x,y,t)|e_1\rangle + \phi_2(x,y,t)|e_2\rangle, \tag{2.4}$$

in which the nuclear wave functions on surfaces 1 and 2 are denoted by $\phi_1(x,y,t)$ and $\phi_2(x,y,t)$, respectively. A common situation in excited-state spectroscopy involving nonradiatively coupled excited potential surfaces is that the radiative coupling of the electronic ground state to one of the zeroth-order excited states is much larger than to the other.[7(a)] For simplicity we assume this to be the case here, although the CI method developed below can be applied to more complicated radiative coupling scenarios with no additional difficulty.

Thus, the initial wave packet, $|\Psi(t=0)\rangle = \phi_g^{(i)}(x,y)|e_1\rangle$, is comprised of the initial (preabsorption) vibrational eigenfunction $\phi_g^{(i)}(x,y)$ of the ground electronic state, "placed" on the radiatively "bright" surface V_1 at time $t=0$. [The appropriateness of this initial state follows from the standard time-domain prescription for computing photodissociation cross sections; cf. Refs. 6(a), 11(b), and below.] The wave function is then propagated according to

$$i\partial_t|\Psi(t)\rangle = H_e|\Psi(t)\rangle. \tag{2.5}$$

The nonradiative coupling results in some leakage of the wave packet to the "dark" surface V_2, so that population develops on both surfaces. This schematized situation is qualitatively related to experimental photofragmentation processes in methyl halides and ICN.[7]

The numerical implementation of TDH via a numerical grid for each spatial dimension, which we will term the time-dependent Hartree grid (TDHG) method, entails the separate propagation of wave packets for each degree of freedom.[2,3] Here, we use TDHG wave-packet dynamics as the foundation on which to construct a CI scheme which naturally incorporates direct correlation effects and accounts for the curve-crossing dynamics. Our original intention was to utilize a two-surface TDHG wave packet of the type considered in Paper II as the zeroth-order approximation, and then build a set of time-dependent orthogonal basis functions on top of it, in the same spirit as the single-surface CI algorithm developed in Paper I. Unfortunately, in the case of nonradiatively coupled multisurface dynamics, some simplicity is lost with this approach. In particular, the "mean-field" coupling term destroys the unitary character of the effective propagation operator which governs the wave-packet evolution in each spatial dimension [cf. Eq. (3.2) of Paper II]. As a consequence, a set of basis functions which is initially orthogonal will not necessarily remain so for the entire propagation interval.

As noted above, it is our desire to preserve the orthogonality of the basis functions over time in order to streamline the computation. To do this we have settled for a less-sophisticated zeroth-order propagation scheme. In particular, the basis wave packets on each surface are propagated by an "optimal" separable single-surface potential. In this way it is entirely straightforward to construct an orthogonal time-dependent set of basis functions on each surface. If the exact wave function is then represented by a superposition of these basis functions, the superposition coefficients evolve according to simple linearly coupled first-order differential equations. These coefficients enable the basis functions to "mix" in order to accurately represent the dynamics on both surfaces and also the transfer of wave-packet amplitude between them. Section III is devoted to the problem of constructing a two-surface CI algorithm, given an arbitrary set of separable single-surface potentials upon which to base it. It will become obvious that the key to successful convergence of such a scheme is to pick a good zeroth-order starting point, i.e., an "optimal" set of single-surface guiding potentials. We have identified two viable candidates for this purpose, and these are set forth in Secs. IV A and IV B, respectively.

III. CONFIGURATION INTERACTION BASED ON SEPARABLE DIABATIC GUIDING POTENTIALS

Let us consider a zeroth-order Hamiltonian of the form

$$H_0(t) = [T_x + T_y + W_1(x,y,t)]|e_1\rangle\langle e_1| + [T_x + T_y + W_2(x,y,t)]|e_2\rangle\langle e_2|, \tag{3.1a}$$

where $W_{1,2}$ are time-dependent separable potentials, i.e., W_1 can be written as

$$W_1(x,y,t) = w_x^{(1)}(x,t) + w_y^{(1)}(y,t) - V_I^1(t) \tag{3.1b}$$

[with an overall constant $V_I^1(t)$ explicitly isolated to make easy contact with the specific forms for $W_{1,2}$ considered in Secs. IV A and IV B below], and likewise for W_2. Note that the initial basis state $X_i^{(1)}(x)Y_j^{(1)}(y)|e_1\rangle$ evolves under $H_0(t)$ into $X_i^{(1)}(x,t)Y_j^{(1)}(y,t)\exp(iS_1)|e_1\rangle$, where $X_i^{(1)}(x,t)$ obeys the one-dimensional (1D) Schrödinger equation,

$$i\partial_t X_i^{(1)}(x,t) = [T_x + w_x^{(1)}(x,t)]X_i^{(1)}(x,t), \tag{3.2}$$

the packets $Y_j^{(1)}$ evolve analogously, and S_1 is a time-dependent phase angle given by $S_1 = \int_0^t dt' V_I^1(t')$. In the same manner, the initial basis state $X_l^{(2)}(x)Y_k^{(2)}(y)|e_2\rangle$ evolves under $H_0(t)$ into $X_l^{(2)}(x,t)Y_k^{(2)}(y,t)\exp(iS_2)|e_2\rangle$, with the time evolution of $X_l^{(2)}$, $Y_k^{(2)}$, and S_2 determined by $W_2(x,y,t)$.

Next, we construct an expansion of the electronic-nuclear wave-packet state $|\Psi(t)\rangle$ which evolves under the full nonradiatively coupled Hamiltonian H_e in Eq. (2.1), utilizing the time-dependent base states just generated, i.e.,

$$|\Psi(t)\rangle = e^{iS_1}\sum_{i,j} a_{ij}^{(1)}(t)X_i^{(1)}(x,t)Y_j^{(1)}(y,t)|e_1\rangle + e^{iS_2}\sum_{l,k} a_{lk}^{(2)}(t)X_l^{(2)}(x,t)Y_k^{(2)}(y,t)|e_2\rangle. \tag{3.3}$$

Note that since all the $X_i^{(1)}$'s are evolved under the *same* 1D Hermitian Hamiltonian [Eq. (3.2)], an initially orthonormal set of $X_i^{(1)}$'s will remain orthonormal throughout the course of the propagation. This is true for the $X_l^{(2)}$, $Y_j^{(1)}$ and $Y_k^{(2)}$ wave-packet sets as well. Hence, if the initial expansion of the wave packet is complete, its time evolution according to Eq. (3.3) remains complete. Moreover, if this representation of $|\Psi(t)\rangle$ is inserted into the Schrödinger equation involving H_e, the superposition coefficients will evolve so as to incorporate effects due to the terms in H_e which cause it to deviate from $H_0(t)$. These "interaction" terms are given explicitly by

$$H_I(t) = H_e - H_0(t) = (V_1 - W_1)|e_1\rangle\langle e_1| + (V_2 - W_2)|e_2\rangle\langle e_2| + G(|e_1\rangle\langle e_2| + |e_2\rangle\langle e_1|). \tag{3.4}$$

Because the electronic-nuclear basis states are orthonormal at all times, the evolution equations obeyed by the coefficients have a very simple structure, namely

$$i\begin{bmatrix}\dot{\mathbf{a}}^{(1)}\\ \dot{\mathbf{a}}^{(2)}\end{bmatrix} = \begin{bmatrix}\mathsf{H}_1 & \mathsf{G}\\ \mathsf{G}^\dagger & \mathsf{H}_2\end{bmatrix}\begin{bmatrix}\mathbf{a}^{(1)}\\ \mathbf{a}^{(2)}\end{bmatrix}, \tag{3.5}$$

where the vector $\mathbf{a}^{(1)}$ is a list of all coefficients $a_{ij}^{(1)}(t)$ associated with the wave packet on surface V_1 (organized into a conveniently indexed linear array), and analogously for $\mathbf{a}^{(2)}$. Furthermore, the time-dependent matrices H_1, H_2 prescribe the coupling between or "mixing" of the various base states. If there are n_x^1 x-basis functions and n_y^1 y-basis functions on surface V_1, the length of $\mathbf{a}^{(1)}$ is $n_x^1 n_y^1 \equiv N_1$, and analogously for $\mathbf{a}^{(2)}$. The matrices H_1 and H_2 are then square matrices of dimension $N_1 \times N_1$ and $N_2 \times N_2$, respectively. Their elements are given explicitly by

$$[\mathsf{H}_\alpha]_{ij,if}(t) = \langle X_i^{(\alpha)}(x,t)\, Y_j^{(\alpha)}(y,t) | \Delta V^{(\alpha)}(x,y,t) | \times X_f^{(\alpha)}(x,t)\, Y_f^{(\alpha)}(y,t) \rangle, \tag{3.6}$$

with $\Delta V^{(\alpha)}(x,y,t) = V_\alpha(x,y) - W_\alpha(x,y,t)$, $\alpha = 1,2$. These matrix elements are independent of the nonradiative coupling, and essentially reflect the inability of an x,y-factorized wave packet to represent the true nuclear motion on one surface or the other even in the absence of nonadiabatic coupling effects.

The matrix G, on the other hand, is solely due to nonradiative coupling. It is of dimension $N_1 \times N_2$ and has matrix elements

$$[\mathsf{G}]_{ij,lk}(t) = \langle X_i^{(1)}(x,t)\, Y_j^{(1)}(y,t) | G(x,y) | X_l^{(2)} \times (x,t)\, Y_k^{(2)}(y,t) \rangle e^{i(S_2 - S_1)}. \tag{3.7}$$

Clearly, G generates transfer of probability amplitude between diabatic surfaces V_1 and V_2.

Since $\mathsf{H}_{1,2}$ are each Hermitian, the overall $(N_1 + N_2) \times (N_1 + N_2)$ coupling matrix on the right-hand side of Eq. (3.5) is Hermitian, and consequently $\mathbf{a}^{(1)*} \cdot \mathbf{a}^{(1)} + \mathbf{a}^{(2)*} \cdot \mathbf{a}^{(2)} = 1$ for all times, i.e., the sum of the probabilities to be on either of the two diabatic surfaces is conserved, as it should be. Moreover, construction of the basis of zeroth-order spatial wave packets $X_i^{(1)}$, $y_j^{(1)}$, etc. is extremely simple, as is the evaluation of all the matrix elements which couple the superposition coefficients in Eq. (3.5). Of course, if the size of the basis needed to converge the solution for $|\Psi(t)\rangle$ becomes too large, these advantages become moot. In practice, the basis wave packets (or equivalently, the guiding potentials $W_{1,2}$) must be chosen judiciously, and this is the subject of the next section.

IV. DIABATIC GUIDING POTENTIALS

A. Bare diabatic potentials

When $G = 0$, a wave packet starting on V_1 is impervious to the existence of V_2. This suggests that we choose W_1 to be the separable time-dependent potential generated by TDH evolution of an appropriate initial wave packet on V_1. An obvious choice for the initial packet is $\phi_g^{(i)}(x,y)$ itself, although other viable options exist.[4] It is reasonable to expect the TDH approximant to W_1 generated in this way to provide a set of basis wave packets capable of representing the net wave packet on surface 1 even when G is "turned on."

Selecting a guiding potential for the dark surface is a more subtle task. However, appeal to the Schrödinger equation results in the conclusion (confirmed by numerical simulations) that a piece of the bright surface wave packet will be shaved off when it goes through the seam where V_1 and V_2 cross. Moreover, in many cases the initial wave packet emerging on the dark surface will nearly be a copy of the bright-surface wave packet at the time when the latter goes through the crossing seam. (As long as the difference $V_2 - V_1$ exceeds the nonradiative coupling strength, little leakage to the dark surface will occur. When the bright-surface packet does begin to leak, in the region of the crossing seam, lowest-order time-dependent perturbation theory indicates that the first signs of leakage will be an approximate, albeit faint, copy of the parent packet.) Thus, our strategy is to use the TDH approximant to the bright-surface wave packet at the time t_c when it goes through the crossing seam to establish an appropriate TDH "guiding" trajectory on the dark surface. Specifically, we propagate $\phi_g(x,y)$ within the TDH approximation on V_1, and label it at time t_c as $X^{(1)}(x,t_c)\, Y^{(1)}(y,t_c)$. We then take the wave packet on the dark surface to be identical at this time, i.e.,

$$X^{(2)}(x,t_c)\, Y^{(2)}(y,t_c) \equiv X^{(1)}(x,t_c)\, Y^{(1)}(y,t_c).$$

To determine the initial wave packet $X^{(2)}(x,0)\, Y^{(2)}(y,0)$ which evolves into $X^{(2)}(x,t_c)\, Y^{(2)}(y,t_c)$ when propagated at the TDH level on V_2, we simply backpropagate $X^{(2)}(x,t_c)\, Y^{(2)}(y,t_c)$ on this surface to $t = 0$. [This is done by complex conjugating $X^{(2)}(x,t_c)\, Y^{(2)}(y,t_c)$, propagating it forward in time through an interval t_c under the TDH approximation, and finally, complex conjugating the resultant wave packet.] TDH propagation of $X^{(2)}(x,0)\, Y^{(2)}(y,0)$ then generates the desired guiding potential W_2.

Having specified an initially factorized wave packet $X^{(\alpha)}(x,0)\, Y^{(\alpha)}(y,0)$, where $\alpha = 1$ or 2, and an appropriate potential surface $V_\alpha(x,y)$, TDH evolution of the initial packet is tantamount to propagation according to the effective separable time-dependent potential

$$\begin{aligned} W_\alpha(x,y,t) = {} & v_{\alpha x}(x) + \langle Y^{(\alpha)}(y,t) | U_I^\alpha(x,y) | Y^{(\alpha)}(y,t) \rangle \\ & + v_{\alpha y}(y) + \langle X^{(\alpha)}(x,t) | U_I^\alpha(x,y) | X^{(\alpha)}(x,t) \rangle \\ & - \langle X^{(\alpha)}(x,t)\, Y^{(\alpha)}(y,t) | U_I^\alpha(x,y) | \\ & \times X^{(\alpha)}(x,t)\, Y^{(\alpha)}(y,t) \rangle. \end{aligned} \tag{4.1}$$

As indicated in Eq. (4.1), these separable potentials are to be inserted directly into the CI prescription developed above in Sec. III. In particular, we can see that for these choices of W_α, the diabatic interaction potentials $\Delta V^{(\alpha)}$ take the simple form

$$\begin{aligned} \Delta V^{(\alpha)}(x,y) = {} & U_I^\alpha(x,y) - \langle X^{(\alpha)}(x,t) | U_I^\alpha(x,y) | X^{(\alpha)}(x,t) \rangle \\ & - \langle Y^{(\alpha)}(y,t) | U_I^\alpha(x,y) | Y^{(\alpha)}(y,t) \rangle \\ & + \langle X^{(\alpha)}(x,t)\, Y^{(\alpha)}(y,t) | U_I^\alpha(x,y) | \\ & \times X^{(\alpha)}(x,t)\, Y^{(\alpha)}(y,t) \rangle. \end{aligned} \tag{4.2}$$

To complete the details of the construction of a set of zeroth-order basis wave packets via the "uncoupled single-surface evolution" strategy, we note that in the numerical work presented below we have chosen to construct the orthonormal basis set as a product of Hermite–Gaussian functions, as was done in Paper I. Moreover, the propagation of the basis wave packets according to the appropriate 1D time-

dependent Schrödinger equation was accomplished via a standard fast Fourier transform (FFT)-based split-operator algorithm.[12]

As will be demonstrated in Sec. V, this "bare diabatic" zeroth-order basis-set strategy works quite well for the direct photodissociation dynamics considered in this work, even when the nonradiative coupling is strong and delocalized. Nevertheless, for more complex dynamics, it may become necessary to have a more sophisticated algorithm for generating a set of time-dependent basis functions that "track" the exact wave-packet motion with sufficient accuracy to ensure rapid convergence of the CI part of the algorithm. For example, the success of the scheme just presented depends on our ability to isolate a single crossing event, and "intuit" how the dark surface wave packet is going to emerge from it. When multiple seam crossings are involved (as in the case of collisionally induced curve crossing, where the scattering wave packet must cross the seam on the way in and on the way out), this strategy obviously has to be modified. Fortunately, the Schrödinger equation is linear, and we anticipate that it will often be possible to separate the evolution of the entire wave packet into a coherent superposition of wave packets, each of which encounter the crossing seam only once. Nevertheless, it would be nice to have an automatic way to generate "optimal" separable diabatic surfaces for arbitrary dynamical scenarios. A step in that direction is taken in the next subsection.

B. Variationally optimized diabatic potentials

In the quantum theory of many-body systems which undergo curve-crossing events, there is a well-known Hartree-type approximation procedure for simplifying the dynamics of secondary or "bath" degrees of freedom by restricting them to have the *same* spatial wave packet (which is sometimes referred to as a "configuration") on both surfaces except for an overall complex scale factor.[13] In such a "single-configuration" or "mean (wave-packet) trajectory" approximation, the nuclear dynamics then proceeds according to a single effective potential (which must be some weighted average of the two relevant diabatic potentials and the nonradiative coupling function; see below), and an overall scale factor sets the probability to be in either electronic state. We can use this idea to determine a single variationally optimized separable effective potential that can be utilized in turn to generate a set of naturally orthogonal basis functions for the purpose of implementing CI corrections to the approximate zeroth-order dynamics.

Specifically, we consider

$$|\Psi(t)\rangle \cong [a_1(t)|e_1\rangle + a_2(t)|e_2\rangle]X(x,t)Y(y,t)e^{iS_t}. \tag{4.3}$$

Appeal to the Frenkel–McLachlan variational principle[14] yields optimized equations of motion for the components $a_{1,2}(t)$, $X(x,t)$, $Y(y,t)$, and S_t. These are most easily stated in terms of the one-dimensional effective potentials

$$\begin{aligned} w_x(x,t) \equiv & |a_1|^2[v_{1x}(x) + \langle u_{1y}\rangle_y u_{1x}(x)] \\ & + |a_2|^2[v_{2x}(x) + \langle u_{2y}\rangle_y u_{2x}(x)] \\ & + 2\,\mathrm{Re}(a_1^* a_2)\langle g_y\rangle_y g_x(x) \end{aligned} \tag{4.4}$$

[here $\langle A\rangle_y = \langle Y(y,t)|A|Y(y,t)\rangle$, etc.], and analogously for $w_y(y,t)$. Furthermore, it is useful to define the "average interaction potential"

$$\begin{aligned} V_I(t) = & |a_1|^2\langle u_{1x}\rangle_x\langle u_{1y}\rangle_y + |a_2|^2\langle u_{2x}\rangle_x\langle u_{2y}\rangle_y \\ & + 2\,\mathrm{Re}(a_1^* a_2)\langle g_x\rangle_x\langle g_y\rangle_y. \end{aligned} \tag{4.5}$$

Hartree-type variational equations of motion for the wave packets $X(x,t)$ and $Y(y,t)$ can be expressed in terms of these quantities as

$$\begin{aligned} i\partial_t X(x,t) &= [T_x + w_x(x,t)]X(x,t), \\ i\partial_t Y(y,t) &= [T_y + w_y(y,t)]Y(y,t); \end{aligned} \tag{4.6}$$

the dynamics of the phase angle S_t is given by

$$\dot{S}_t = V_I(t); \tag{4.7}$$

and the coefficients $a_{1,2}(t)$ evolve according to

$$\begin{aligned} i\begin{bmatrix}\dot{a}_1\\ \dot{a}_2\end{bmatrix} &= \begin{bmatrix}\langle V_1(x,y) - W(x,y)\rangle_{x,y} & \langle g_x\rangle_x\langle g_y\rangle_y \\ \langle g_x\rangle_x\langle g_y\rangle_y & \langle V_2(x,y) - W(x,y)\rangle_{x,y}\end{bmatrix} \\ &\quad \times \begin{bmatrix}a_1\\ a_2\end{bmatrix}. \end{aligned} \tag{4.8}$$

[Here $\langle A\rangle_{x,y} = \langle X(x,t)Y(y,t)|A|X(x,t)Y(y,t)\rangle$, and $V_1(x,y)$ is the *complete* diabatic potential surface associated with electronic state $|e_1\rangle$ given in Eq. (2.3).]

Note that since this strategy requires the diabatic guiding potentials for both surfaces and the corresponding central wave-packet trajectories to be identical, it will not yield asymptotically correct zeroth-order (pre-CI) dynamics unless the diabatic potential surface V_1 and V_2 are asymptotically identical to within an overall constant. In the numerical work presented in Sec. V we employ potentials with this property [in particular, the asymptotic vibrational potentials $v_{\alpha x}(x)$, $\alpha = 1,2$, are chosen to be the same]. In more general circumstances, it may be wise, in order to guarantee asymptotic stability of the exiting wave packets, to transform to an interaction picture representation[15] in which the asymptotic motion on surfaces V_1 and V_2 has been removed.

Once the effective potential $W(x,y) = w_x(x,t) + w_y(y,t) - V_I(t)$ has been determined, CI corrections can be built as discussed in Sec. III. Note that since $W_1 = W_2 = W$ in this scheme, the same effective separable potential is used to generate the (same) set of time-dependent orthonormal basis functions on surfaces V_1 and V_2. Corrections to this "single-configuration" two-surface Hartree wave-packet dynamics are then achieved by mixing the basis superposition coefficients in the manner described in Sec. III.

V. NUMERICAL APPLICATION

To illustrate the utility of our coupled-surface CI algorithm we have studied photodissociation in a model involving two degrees of freedom which evolve according to Beswick–Jortner[8] (BJ) type potential surfaces, i.e.,

$$V_\alpha(x,y) = A_\alpha \exp[-B_\alpha(y - C_\alpha x)] + \tfrac{1}{2}K_\alpha x^2 + V_\alpha^{(0)}. \tag{5.1}$$

The BJ model provides a qualitative description of the dissociation dynamics of a triatomic molecule such as ICN in the absence of overall rotation. In particular, the y coordinate describes the bond which has been broken by direct electronic excitation (e.g., the distance between I and the CN center of mass) and the x coordinate describes the internal vibration (e.g., the CN vibration) which is excited in the process. The form of the nonradiative coupling function is at present not well understood for most polyatomic curve-crossing systems. In Paper II we studied the effects of coupling functions which are localized vs nonlocalized in the crossing region, and found that a nonlocalized coupling of the form $G(x,y) = g_0 \exp[-\beta(y-y_0)]$ produced particularly complicated wave-packet dynamics. Hence to challenge the proposed CI method, such a nonradiative coupling function has been adopted for the numerical work described below.

Computation of partial cross sections for dissociation into specified asymptotic fragment states requires accurate propagation of the wave packet over the full course of the photodissociation event. Specifically, the cross section to result in vibrational state v on diabatic surface $\alpha = 1,2$ is obtained from the asymptotic evolution of the wave packet according to[11(c)]

$$\sigma_\alpha^{(v)}(\omega_L) = |\langle k_\alpha^{(v)}(y)|\langle \chi_\alpha^{(v)}(x)|\phi_\alpha(x,y,t\to\infty)\rangle|^2, \tag{5.2}$$

where $\chi_\alpha^{(v)}$ is the vth asymptotic vibrational eigenfunction on surface V_α, and $|k_\alpha^{(v)}\rangle$ is an appropriately normalized plane-wave state with wave vector $k_\alpha^{(v)}$ determined by conservation of energy. [For the class of two-dimensional Hamiltonians considered in this paper $E_g^{(i)} + \omega_L = \epsilon_\alpha^{(v)} + k_\alpha^{(v)2}/2m_y$, where $E_g^{(i)}$ is the vibrational energy eigenvalue associated with $\phi_g^{(i)}(x,y)$, the initially prepared vibrational state on the ground electronic surface, ω_L is the incident laser frequency, and $\epsilon_\alpha^{(v)}$ the vibrational energy eigenvalue associated with the asymptotic vibrational fragment state $\chi_\alpha^{(v)}(x)$.] In the commonly encountered situation alluded to above where only one of the excited diabatic surfaces is radiatively coupled to the ground electronic surface, the partial cross sections for photodissociation onto the other, radiatively "dark" excited surface are particularly sensitive to wave-packet propagation errors. Again, to challenge our CI method, we will concentrate primarily on the quality of the dark-surface partial cross sections which it can provide.

In Paper II the coupled two-surface TDHG approximation was found to be remarkably successful at tracking the curve-crossing dynamics of an initially Gaussian wave packet. Even bifurcations in the exiting wave packets (a common occurrence in the case of nonlocal nonradiative coupling) were well accounted for by TDHG level dynamics. However, we know from previous work in Paper I [and also Ref. 3(b)] that the TDHG method has more difficulty propagating spatially extended initial states which can arise when some degrees of freedom are vibrationally excited. For this reason, we focus on initially vibrationally excited states in the tests reported here. As anticipated, simple TDHG dynamics can yield inaccurate partial cross sections for such initial states, particularly with regard to dissociation on the radiatively dark diabatic surface. As we shall demonstrate, errors in the TDHG dynamics can easily be corrected using the CI scheme proposed in Sec. III.

TABLE I. Parameters used to generate the potential-energy surfaces and the nonradiative coupling fuction.

Potential parameter ($\alpha = 1,2$)				
A_α	B_α	C_α	K_α	$V_\alpha^{(0)}$
13.71	0.4547	0.9850	43.28	4.0
34.04	0.4547	0.9850	43.28	0.0
g_0		β		y_0
5.7		0.668		0.0

The computations reported below are for the same basic system considered in Paper II. Specifically, we set the mass pertaining to each coordinate equal to 1 and the potential parameters as indicated in Table I. We chose the nonradiative coupling strength to achieve about 50% transmission to the dark surface and focused on the case that the initial wave function corresponds to two quanta of excitation, i.e., $v = 2$ in the "CN stretch." The parameters x_s, y_s, which set the starting location of the wave packet in the x and y coordinates, were set to 0.665 and 1.5, respectively. In Fig. 1, we present snapshots of the probability density of the wave packet on the dark surface when the propagation is performed using the coupled-surface TDHG approximation of Paper II. [It should perhaps be emphasized that all "TDHG" results displayed in the figures are based on the coupled-surface TDHG algorithm of Paper II, while all "CI" results are based on the two-surface TDHG-CI algorithm developed in this paper, which utilizes separable *single*-surface guiding potentials to generate the basis functions appropriate to each diabatic potential.] As observed in that

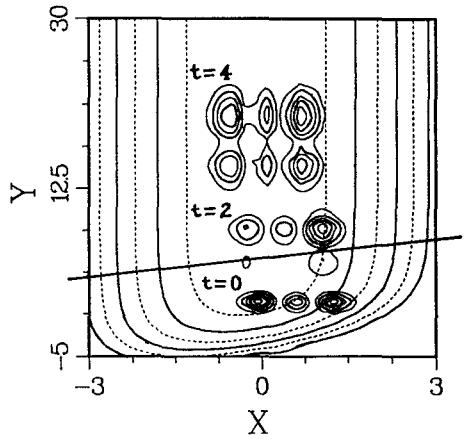

FIG. 1. TDHG contour plot of dark-surface wave-packet probability densities for times $t = 2$ and 4 on the dark surface, V_2. The initial wave packet on *bright* surface, V_1, is also indicated for reference. (The dark-surface wave packet is identically zero at $t = 0$.) The x and y coordinates represent the bound and dissociative degrees of freedom, respectively. The straight line denotes the $V_1 - V_2$ crossing seam.

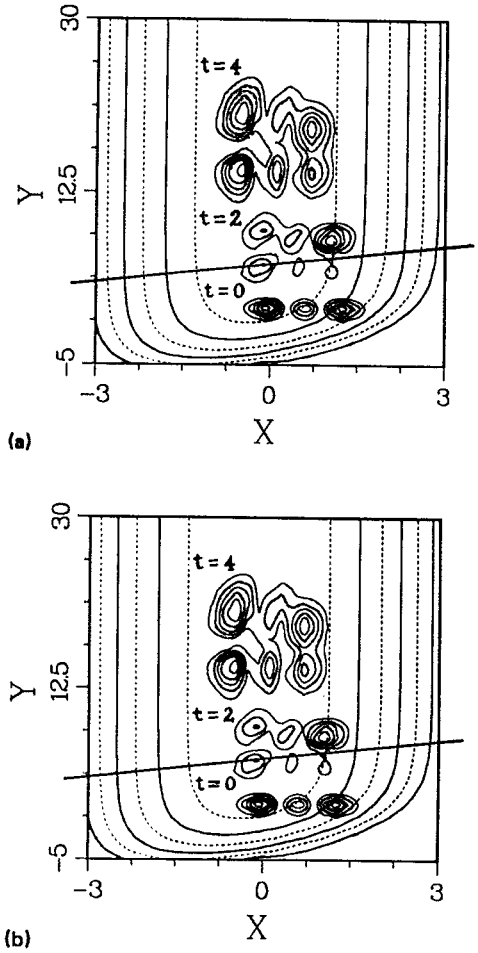

FIG. 2. Probability densities, as in Fig. 1, comparing exact dark-surface probabilities at times $t = 2$ and 4 (solid) vs those for (a) CI scheme A (CI-A) and (b) CI scheme B (CI-B) (dashed lines). The basis set employed is indicated in Table II.

work, the dark-surface wave packet bifurcates, and furthermore, the TDHG packet retains a rigid orientation along the x and y axes. In Figs. 2(a) and 2(b) we depict the analogous probability densities obtained from our CI methods outlined in Sec. IV A (scheme A) and Sec. IV B (scheme B), respectively, which are compared to exact results obtained via two-dimensional (2D) split-operator FFT propagation.[12] There are two important features to note concerning Fig. 2. First, as it evolves the exact wave packet becomes twisted in such a way that it cannot be accurately represented by a single factorized ("rigid") TDHG packet. Second, our CI algorithm,

TABLE II. Number of basis functions (BF's) used for calculations shown in Figs. 2 and 3. CI-A stands for the scheme developed in Sec. IV A, and analogously, CI-B is for that in Sec. IV B.

	Bright surface		Dark surface	
	CI-A	CI-B	CI-A	CI-B
x BF's	5	5	6	6
y BF's	8	7	14	14

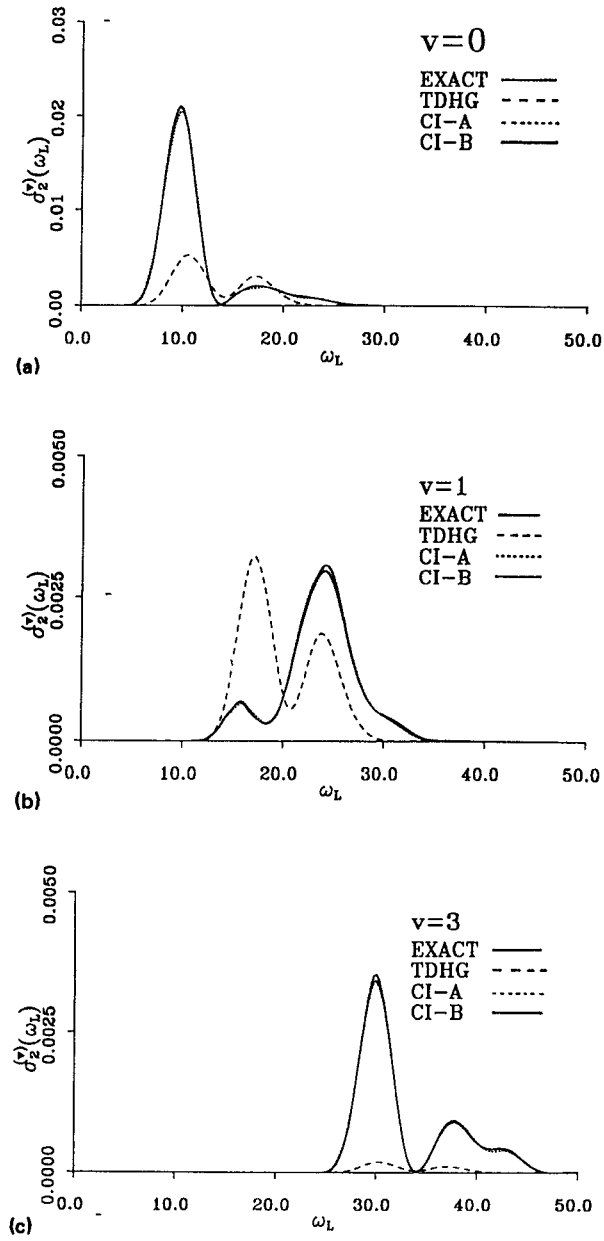

FIG. 3. Exact (solid), CI-B (solid), CI-A (dotted), and two-surface TDHG (dashed line) partial cross sections for population of the asymptotic vibrational eigenstates (a) $v = 0$, (b) $v = 1$, and (c) $v = 3$ on the dark potential-energy surface V_2, as a function of incident laser frequency ω_L.

implemented with guiding diabatic potentials generated by the strategy of either scheme A or scheme B, is capable of representing the required wave forms without undue effort. Close examination reveals that the numerical results obtained from the CI variations A and B are not quite identical. In particular, the rate of convergence of the two schemes differs slightly, as discussed more fully in Sec. VI. However, the final results obtained from the two methods are of comparable quality. Certainly, the converged wave-packet trajectories obtained with a "large" number of basis functions (cf. Table II for details) are indistinguishable at the level of resolution characterizing Fig. 2.

In Fig. 3 we present partial cross sections on the dark

surface converged via "large" basis CI computations and compare these to exact and TDHG results. As can be seen, both CI algorithms yield results which are very close to the exact ones (extracted from the numerical grid integration scheme described above), while the analogous TDHG results are poor. In general, variation *B* performs slightly better than *A*, but the agreement is sufficiently good in both cases to be termed "quantitative." Even though we have termed these "large-basis" calculations, the computational effort is still small compared to that required for exact 2D FFT integration. We have not tried to fully optimize the performance of either the split-operator FFT or TDHG-CI codes, but for the versions which were utilized in these calculations, we estimate conservatively that the TDHG-CI code applied to the "large" basis set indicated in Table II is 3–4 times faster than the 2D split-operator FFT.

An important feature of our algorithm is the flexibility to concentrate effort on the hardest degrees of freedom or diabatic surface(s). In the present calculation we can see from Table II that to get a very accurate bright surface wave packet requires 35 basis functions (5 for the *x* coordinate and 7–8 for the *y* coordinate), but that the more elaborate motion on the dark surface requires 84 basis functions for CI scheme *A* and 70 for scheme *B*. In the same spirit, we are free to choose different numbers of basis functions on different degrees of freedom (e.g., 6 vs 14 on the dark surface for *x* and *y*, respectively). We expect this flexibility to concentrate numerical effort where it is required will prove to be *crucial* in applications to multidimensional systems.

TABLE III. Same as Table II, but for the calculations shown in Figs. 4–7.

	Bright surface		Dark surface	
	CI-*A*	CI-*B*	CI-*A*	CI-*B*
x BF's	3	3	3	3
y BF's	7	7	7	7

It is also interesting to explore the accuracy of these CI methods when a smaller number of basis packets are utilized. This is an important issue because it may be possible using small basis sets to obtain semiquantitative results at a very low cost. In Fig. 4 we show results analogous to those

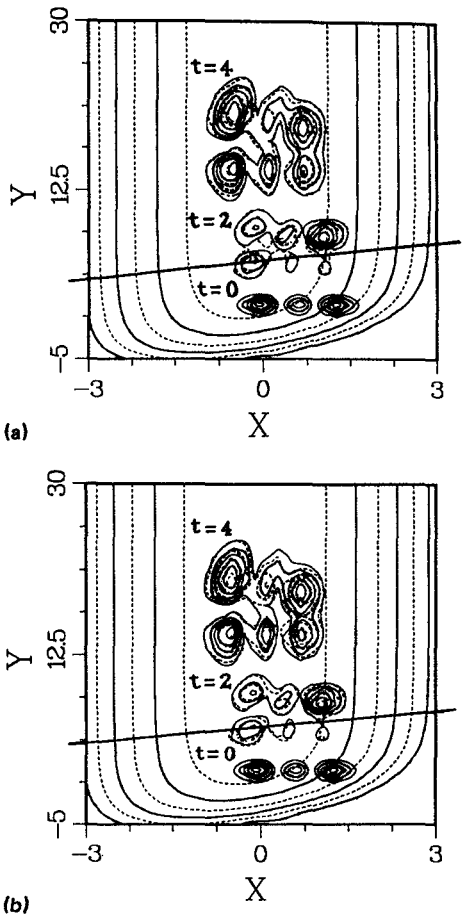

FIG. 4. As in Fig. 2, but using a smaller basis set (see Table III).

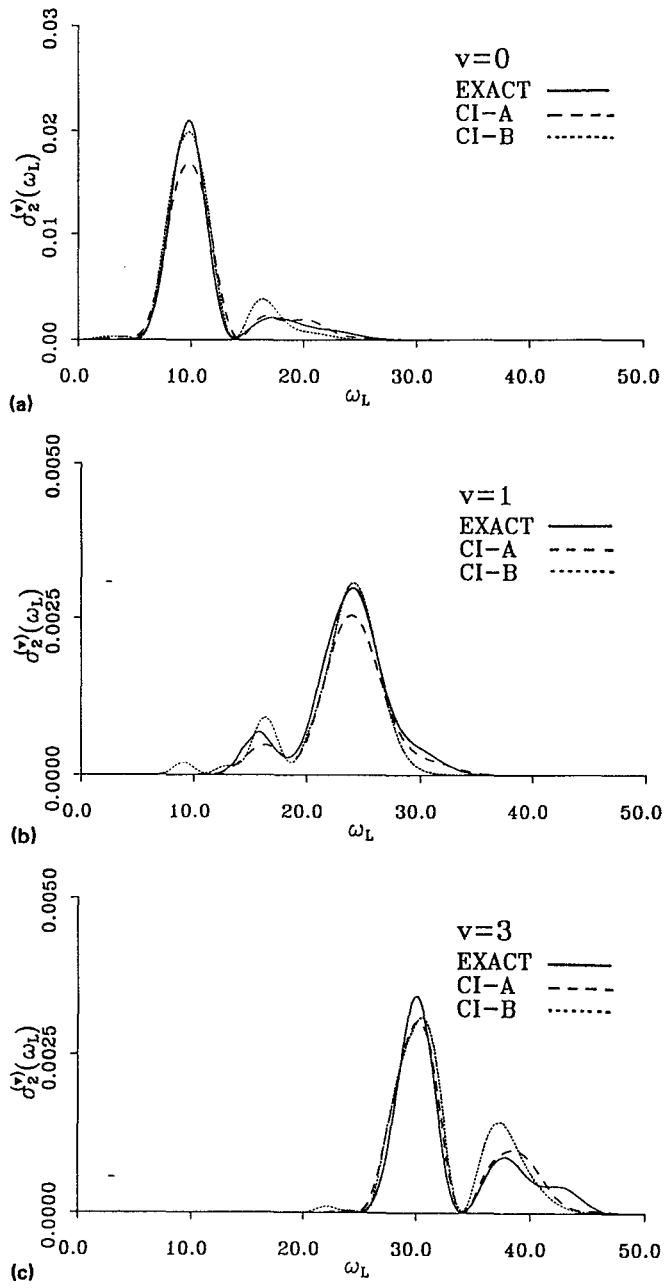

FIG. 5. As in Fig. 3, but using a smaller basis set (see Table III).

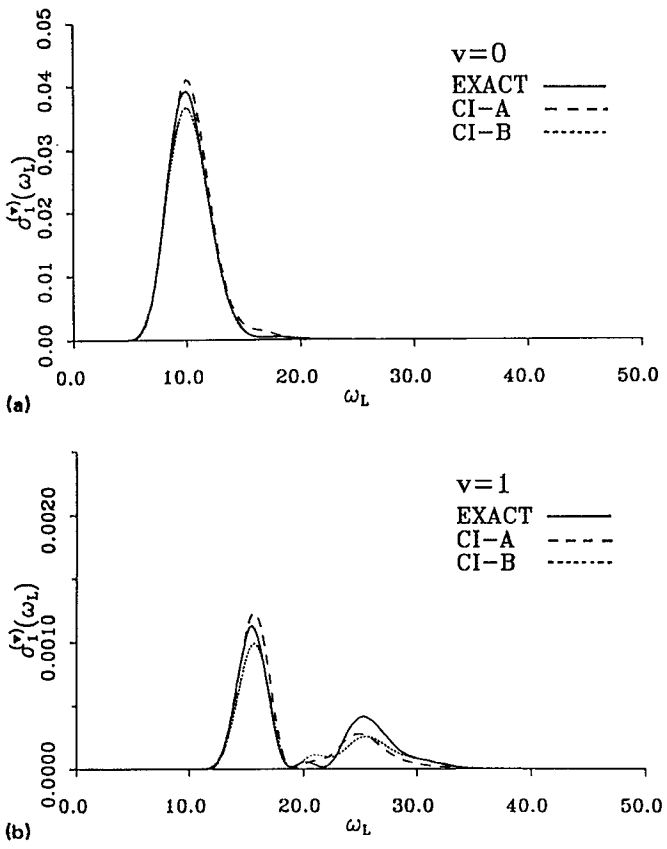

FIG. 6. Bright-surface partial cross sections extracted from the small basis-set calculation specified in Table III. Exact (solid line) and TDHG (dotted line) results are compared for final vibrational states (a) $v = 0$ and (b) $v = 1$.

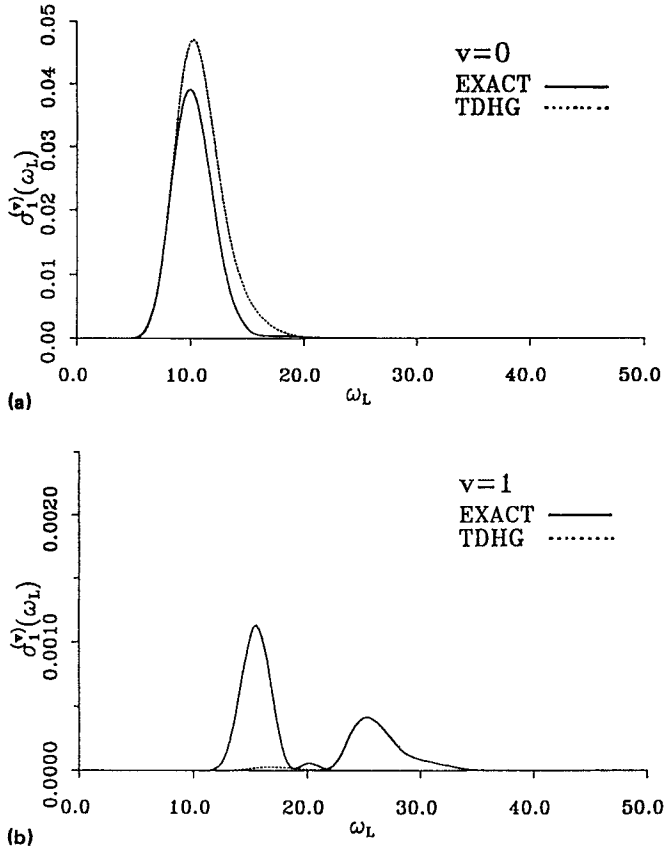

FIG. 7. Bright-surface partial cross sections extracted from the small basis-set calculation specified in Table III. Exact (solid line), CI-*A* (dashed line), and CI-*B* (dotted line) results are compared for final vibrational states (a) $v = 0$ and (b) $v = 1$.

contained in Fig. 2, except that they were obtained with the "small-basis" set described explicitly in Table III. It can be seen from the probability density plots in Fig. 4 that the essential distortions of the dark-surface wave packet are already contained in these small-basis CI computations. Obviously, these results are not converged to the same level as the large-basis CI trajectory in Fig. 2, and consequently the partial cross sections extracted from the small-basis wave packet are not expected to be as accurate as their large-basis counterparts. This is, in fact, the case, as Fig. 5 shows. Although there are small discrepancies between small-basis CI and exact results, the improvement over TDHG-level results obtained with this modest amount of CI is dramatic (cf. Fig. 3). Considering that the small-basis CI calculation runs five times faster than the large-basis counterpart used to generate Figs. 2 and 3, the virtue of small-basis CI corrections is clear.

Small-basis CI results for the bright-surface partial cross sections, presented in Figs. 6 and 7, reinforce this conclusion. We expect these quantities to be somewhat less delicately dependent on the hopping of wave amplitude between the two diabatic surfaces, and indeed, small-basis CI does a good job in accounting for them, as Fig. 7 shows. Nevertheless, the effects of CI corrections are often substantial, as the failure of TDHG in Fig. 7(b) indicates.

VI. DISCUSSION AND CONCLUSIONS

In recent years the time-dependent Hartree approximation[14] has been established as an important tool for studying many-body quantum dynamics.[2,3,9] It has major computational and interpretive advantages. Computationally, it reduces the scaling of effort from an exponential to a nearly linear function of spatial dimensionality. At the same time, the factorization of the overall system wave packet into single-degree-of-freedom pieces allows easy visualization of many-body quantum dynamics.

Nevertheless, the TDH approximation can fail qualitatively in situations where correlation effects become sufficiently strong.[2,3(b),4,6(c),16] We have shown in this paper that spatially extended wave packets moving on nonradiatively coupled diabatic potential surfaces can stymie TDHG methods. Clearly, the ability to compute strongly correlated wave-packet dynamics for multidimensional curve-crossing problems is required in order to successfully model many experimentally interesting scenarios. The coupled-surface TDHG-CI algorithm introduced in this work appears to hold some promise in this regard.

As noted in the Introduction, the idea of correcting for the deficiencies of a Hartree factorization ansatz by representing the exact system wave function as a superposition of products of single-coordinate functions is not new. This idea

has been extensively developed in CI methods for computing electronic structure of atoms and molecules.[5] It has also been utilized in time-dependent wave-packet dynamics applications, although to a much lesser extent. Most extant wave-packet CI algorithms other than the one introduced in Paper I utilize projection operators that assign different parts of the Hilbert space to different functions. Such algorithms are often referred to as MC-TDSCF [Refs. 2(a) and 16] or MC-TDH,[6(c)] where the abbreviation MC stands for "multiconfiguration" (a "configuration" being a single factorized TDH wave packet).[17] It is difficult to obtain accurate results from a highly restricted set of TDH-type configurations since considerable intuition is required to pick the projection operators. The other alternative is to use many configurations to "forcibly" span the relevant Hilbert space. A rather general formal procedure along these lines has recently been given by Meyer, Manthe, and Cederbaum.[6(c)] However, the prescribed equations of motion are quite complicated. The CI algorithm developed in Paper I sacrifices flexibility in the basis functions in return for very simple evolution equations for both the basis wave packets and the mixing coefficients. One of the strengths of this strategy is that it can be extended in a practical way to more complicated situations, such as the case of wave-packet motion on coupled potential surfaces studied herein.

A critical issue in the construction of the coupled-surface CI scheme developed in this work is the choice of "optimal" zeroth-order diabatic guiding potentials which are used to generate orthonormal traveling TDH-type basis wave packets on each diabatic surface. We introduced two possibilities for these potentials. It is interesting to compare their performance as a guide to developing other alternatives. Scheme *A*, which used diabatic potentials based completely on single-surface motion, appears natural when the nonradiative coupling is weak, since it correctly anticipates what the coupled-surface motion will look like in this limit. (The central wave packet on the dark surface is generated so that it is equal to its bright-surface counterpart when the latter goes through the diabatic potential crossing seam.) In general, it appears to be more accurate than scheme *B* when a very small basis is utilized.

In the latter scheme, a single effective separable diabatic potential guides the (same set of) wave packets on both surfaces. This "mean (wave-packet) trajectory" potential is determined by substituting a simple trial function of the appropriate form into the McLachlan variational principle. The *resultant* basis is somewhat less natural for describing weak or highly localized coupling effects (since the bright- and dark-surface basis wave packets cannot "go their separate ways" after the bright-surface wave packet goes through the crossing seam). Hence it is somewhat poorer when only a very small number of basis packets are employed. However, as more packets are added, the superposition of packets obtained within scheme *B* becomes flexible enough to account for the fact that true wave packets on the two surfaces are not completely "slaved" to each other. Furthermore, the fact that some intersurface coupling is included via the preliminary "mean wave-packet trajectory" variational computation enables the basis packets to partially adjust to the nonradiative coupling, and consequently, once scheme *B* begins to converge to the exact result, it does so more rapidly than scheme *A*.

In terms of flexibility, we should remember that the diabatic guiding potentials of scheme *A* are easy to construct and naturally describe the asymptotic motion of the exiting wave packets when the nonradiative coupling has gone to zero. The only difficulty could come when the wave packets go through the crossing seam multiple times, as discussed in Sec. IV A. The variationally determined diabatic guiding potentials of scheme *B*, on the other hand, have the advantage that the variational principle eliminates all guesswork. For potentials of the kind considered here, the determination of optimal guiding potentials is straightforward and asymptotically stable. However, for more general potentials, complications with regard to asymptotic post-dissociation stability may arise unless more elaborate procedures are developed.

The basic difficulty with the coupled-surface CI method developed herein is that it relies strongly on the TDH approximation for its foundation. In cases where TDH-level dynamics is qualitatively reasonable, our CI algorithm seems quite sensible, but in cases where TDH-level solutions are qualitatively misleading, the same algorithm will become inefficient. (The single-surface version of this CI algorithm[4] suffers from the same problem.) Several possibilities for improving upon the zeroth-order dynamics are naturally suggested.

The utilization of partially correlated (orthonormal) zeroth-order basis functions is worth investigating. For example, it may be possible to use the variational generator approach of Kucar and co-workers[18] to allow some degrees of freedom to rotate among themselves within the restrictions imposed by a convenient variational trial function and still preserve the orthonormality of the partially correlated basis functions. Also, the incorporation of feedback between superposition coefficients and basis functions remains to be explored. In the implementations of our CI schemes pursued to date, the basis coefficients respond to the zeroth-order TDH-type wave-packet motion, but *not vice versa*. If a way could be found to enable the basis functions to adjust to the instantaneous shape of a multiconfiguration wave packet (without compromising the orthonormality of the basis functions), erosion of the accuracy of the zeroth-order basis functions could, in principle, be substantially reduced. Finally, we have observed that although the list of basis coefficients becomes long as the number of excitations included in the basis increases, most coefficients are very nearly zero. It should be possible to sift out the instantaneously unimportant basis functions, and thereby reduce the effective basis size. Clearly, there are many directions along which the basic ideas introduced here can be expanded, and many applications to multidimensional molecular systems which lie ahead.

ACKNOWLEDGMENTS

J. C.-M. gratefully acknowledges a grant from the Ministerio de Educacion y Ciencia of Spain and the Fulbright

Comission. R. D. C. wishes to thank the National Science Foundation (Grant No. CHE-9101432), the Donors of the Petroleum Research Fund, administered by the American Chemical Society and the Camille and Henry Dreyfus Foundation for financial support, and the Pittsburgh Supercomputing Center where many of the calculations were carried out.

[1] For a cross section of recent work in this area, see Comput. Phys. Rep. **63** (1991).

[2] (a) R. Kosloff, J. Phys. Chem. **92**, 2087 (1988); (b) R. H. Bisseling, R. Kosloff, R. B. Gerber, M. A. Ratner, L. Gibson, and C. Cerjan, J. Chem. Phys. **87**, 2760 (1987); (c) R. Alimi and R. B. Gerber, Phys. Rev. Lett. **64**, 1453 (1990); (d) Z. Kotler, A. Nitzan, and R. Kosloff, Chem. Phys. Lett. **153**, 483 (1988).

[3] (a) M. Messina and R. D. Coalson, J. Chem. Phys. **90**, 4015 (1989); (b) R. D. Coalson, Chem. Phys. Lett. **165**, 443 (1990); (c) M. Messina and R. D. Coalson, J. Chem. Phys. **92**, 5297 (1990); (d) **92**, 5712 (1990); R. D. Coalson and M. Karplus, *ibid.* **93**, 3919 (1990).

[4] J. Campos-Martinez and R. D. Coalson, J. Chem. Phys. **93**, 4740 (1990).

[5] See, for example, A. Szabo and N. S. Ostlund, *Modern Quantum Chemistry* (MacMillan, New York, 1982).

[6] (a) S.-Y. Lee and E. J. Heller, J. Chem. Phys. **76**, 3035 (1982); (b) R. D. Coalson and M. Karplus, Chem. Phys. Lett. **90**, 301 (1982); (c) H.-D. Meyer, U. Manthe, and L. S. Cederbaum, *ibid.* **165**, 73 (1990).

[7] (a) K. Q. Lao, M. D. Person, P. Xayariboun, and L. J. Butler, J. Chem. Phys. **92**, 823 (1990); (b) J. F. Black, J. R. Waldeck, and R. N. Zare, *ibid.* **92**, 3519 (1990).

[8] J. A. Beswick and J. Jortner, Chem. Phys. **24**, 1 (1977).

[9] J. R. Waldeck, J. Campos-Martinez, and R. D. Coalson, J. Chem. Phys. **94**, 2773 (1991); *ibid.* **95**, 1430 (E) (1991).

[10] See F. T. Smith, Phys. Rev. **179**, 111 (1969) for a discussion of how to construct diabatic potentials from Born–Oppenheimer adiabatic potentials.

[11] For extensive discussions about wave-packet evolution on nonradiatively coupled diabatic potential surfaces, see (a) R. D. Coalson and J. L. Kinsey, J. Chem. Phys. **85**, 4322 (1986); (b) R. D. Coalson, Adv. Chem. Phys. **73**, 605 (1989); (c) J. Chem. Phys. **86**, 6823 (1987).

[12] M. D. Feit, J. A. Fleck, Jr., and A. Steiger, J. Comput. Phys. **47**, 412 (1982). For a more general discussion of grid propagation technology see Ref. 2(a).

[13] For applications of the "mean trajectory approximation" in which the nuclear motion is treated via classical trajectories, see S. Sawada, A. Nitzan, and H. Metiu, Phys. Rev. B **32**, 851 (1985); A. E. Depristo, Surf. Sci. **137**, 130 (1984); for applications in which the nuclear motion is treated via wave-packet dynamics, see G. Wahnstrom, B. Carmeli, and H. Metiu, J. Chem. Phys. **88**, 2478 (1988); and Ref. 2(d).

[14] J. Frenkel, *Wave Mechanics* (Oxford University, Oxford, 1934); A. D. McLachlan, Mol. Phys. **8**, 39 (1964).

[15] See, for example, G. Baym, *Lectures on Quantum Mechanics* (Benjamin, London, 1969), Chap. 12.

[16] Failure of the TDH approximation when applied to multidimensional tunneling problems are pointed out by N. Makri and W. H. Miller, J. Chem. Phys. **87**, 5781 (1987).

[17] The nomenclature in the wave-packet dynamics literature is unfortunately not standardized. Hence, the term MC-TDSCF as used by some authors has a meaning somewhat different from the one just explained. In particular, Kotler *et al.* in Ref. 2(d) use MC-TDSCF to indicate a two-surface wave packet [cf. Eq. (2.4)] in which the spatial wave packet on each surface is of TDH type and there is a different one-dimensional wave packet associated with each spatial coordinate of each electronic state. Their MC-TDSCF wave packet is thus what we call a "two-surface TDHG" wave packet in Paper II, and we utilize it here as a foil for the more sophisticated TDHG-CI method developed in this paper (cf. Figs. 3 and 7).

[18] J. Kucar, H.-D. Meyer, and L. S. Cederbaum, Chem. Phys. Lett. **140**, 525 (1987); H.-D. Meyer, J. Kucar, and L. S. Cederbaum, J. Math. Phys. **29**, 1417 (1988).